Heliyon 11 (2025) e42369

Contents lists available at ScienceDirect

Heliyon

journal homepage: www.cell.com/heliyon

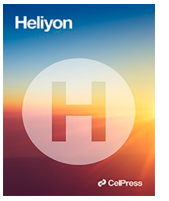

Research article

One pot oxidative ethyl acetate synthesis using palladium activated SBA-15 type catalysts

Yesim Gucbilmez [a,*], Ibrahim Calis [b]

[a] Department of Chemical Engineering, ESTU, Eskisehir, 26555, Turkey
[b] Central Research Lab, Bartin University, Bartin, 74100, Turkey

ARTICLE INFO

Keywords:
SBA-15
Pd-SBA-15
One pot oxidative synthesis
Ethyl acetate
Partial oxidation

ABSTRACT

Ethyl acetate, an important fuel additive and green solvent, was produced through one pot oxidative synthesis of EtOH using palladium incorporated SBA-15 type catalysts synthesized by the impregnation (IMP) method. This was the first time these catalysts were used in this reaction at mild EtOH vaporization conditions (35 °C). XRD, N_2 physisorption, SEM, CO chemisorption and TPR methods were used to characterize the as-synthesized catalysts. All the catalysts were found to maintain the SBA-15 semi-crystalline structure with high BET surface areas (626–665 m^2/g), and high pore volumes (0.93–0.95 cm^3/g) and metal distributions in the range of 24–29 %. The optimum Pd/Si molar ratio in solution was found to be 0.03 and the corresponding catalyst was tested in the one pot oxidative synthesis of ethyl acetate at different reaction temperatures and different O_2/EtOH molar ratios. The maximum ethyl acetate yield was obtained as 0.25 at 200 °C and 1 atm at an O_2/EtOH molar ratio of 0.5 and space velocity of 2206 h^{-1} using this catalyst. The fact that the best yield was obtained at mild conditions of temperature and pressure decreased the energy requirement of the ethyl acetate production process. In addition, in Turkey, bio-ethanol is produced from sugar beet pulp, thus, the oxidative synthesis of ethyl acetate can be made more sustainable by using sugar beet based ethanol.

1. Introduction

Ethyl acetate is used as a green solvent in the manufacturing processes of coatings, paints, resins [1], as an additive in the development of various flavors and fragrances [2,3], and as an oxygenated fuel additive [4,5]. When ethyl acetate is blended with gasoline, it is seen that the GHG emissions reduce and there is a very low thermal energy difference between the blend and pure gasoline. When it is added to ethanol-gasoline blends, on the other hand, it increases the octane number and stability of the fuel and it does not negatively affect the volatility of the fuel blend [4,5]. Presently, ethyl acetate is produced from petrochemical sources through energy-demanding and unsustainable processes. The traditional Fischer-Speier esterification method, which involves equilibrium reactions, requires significant energy for the high temperatures involved and for continuously removing water from the system. This energy demand increases the production cost of ethyl acetate [6–8]. Another pathway for ethyl acetate synthesis is the Tishchenko reaction of acetaldehyde in which aluminium triethoxide is used as the catalyst [9,10]. In this reaction, a yield of 61 % can be obtained at −20 °C by the addition of aluminum triethoxide to the reaction mixture [9]. The Tishchenko reaction can be performed using two different pathways: the dehydrogenative route and the oxidative route. The dehydrogenative route involves the use of copper or

* Corresponding author.
E-mail address: ygucbilmez@eskisehir.edu.tr (Y. Gucbilmez).

https://doi.org/10.1016/j.heliyon.2025.e42369
Received 16 January 2025; Received in revised form 26 January 2025; Accepted 28 January 2025
Available online 29 January 2025

palladium-based catalysts, while the oxidative route utilizes PdO activated catalysts. The dehydrogenative route for ethyl acetate production generates by-products in addition to ethyl acetate and hydrogen, creating a complex mixture that is costly and difficult to purify. In the oxidative route, however, the purification of ethyl acetate is straightforward and the used catalysts are highly stable [10]. In the last years, novel methods such as electrocatalytic reactions, enzymatic reactions, microbial fermentation, reactive distillation, and reactions with membranes and zeolites have been used to produce ethyl acetate. Electrocatalytic production is the synthesis of ethyl acetate using electricity driven reactions. Electrocatalysts can increase the rate, efficiency, and selectivity of the chemical reactions and renewable electricity can be used as the energy source, however, the present electrocatalysts are inadequate and research should be carried out to develop electrocatalysts with enhanced performance [11]. Considering enzymatic reactions, Hwang and Park [12] produced ethyl acetate at 25 °C reacting gaseous ethanol and acetic acid using a lipase from Porcine Pancreas. They investigated the effect of different moisture contents of the lipase. They found that as the moisture content increased there was a decrease in ethyl acetate production, since water had an adverse effect on the equilibrium of the reaction as stated by Carta et al. [13]. Aghazadeh et al. [14] studied the production of ethyl acetate using bioethanol fermentation. They found that addition of acetic acid significantly inhibited the adapted, genetically modified and wild-type *S. cerevisiae*. To reduce the inhibition effect, they used liquid–liquid extraction to remove the acetic acid and evaporation to recover the extraction solvent. This modified process was found to have a significant increase in ethanol specific production rate and ethanol yield. Šulgan et al. [15] used reactive distillation to produce ethyl acetate trying four different process configurations. They used ASPEN PLUS and the thermodynamic model NTRL-HOC for the modelling studies. They found that the configuration of reactive distillation column with an auxiliary reaction gave the best results. Ethyl acetate conversion significantly increases when reactive distillation is used, however, the design of the process remains a challange due to the difficulties in modelling and scaling-up [16]. For process intensification and reduction of energy cost, zeolites and membranes were also successfully used in the production of ethyl acetate [17,18]. In this study, the oxidative route is utilized and effect of reaction parameters on the ethyl acetate selectivity and yield are investigated.

2. Materials and methods

"Rigaku Ultima-IV diffractometer with CuKα = 0.15406 nm radiation was used to obtain the XRD patterns of the catalysts in the 2Θ range of 1–80°. N_2 physisorption experiments were carried out with the Micromeritics ASAP 2020 system. Before the experiments, approximately 0.200 g of sample was degassed at 150 °C and in high vacuum for 10 h. Brunauer-Emmett-Teller surface area (S_{BET}), total pore volume (V_t), Barrett-Joyner-Halenda (BJH) average pore diameter (d_{BJH}), BJH mesoporous surface area ($S_{m,BJH}$), Dubinin-Radushkevich microporous surface area ($S_{\mu,DR}$), Dubinin-Radushkevich micro pore volume ($V_{\mu,DR}$) and the Dubinin-Astakhov micro pore diameter (d_{DA}) values of all samples were obtained using the N_2 physisorption data. Zeiss Supra 50 VP Microscope with 20 kV accelerating voltage and 7.5–10.5 mm working distance was used to obtain the SEM images. In order to obtain clear images, the powder samples were dispersed in ethanol, and the resulting suspension was dripped onto the glass attached to a carbon tape and dried. Images of the samples were taken at 5000× and 20000× magnifications. Micromeritics Chemisorb 2720 system equipped with a thermal conductivity detector (TCD) was used to carry out the CO chemisorption studies. During the analyses, 0.1 mL of carbon monoxide gas (CO) was injected into the system as impulses at 5 min time intervals until the TCD signal was constant. Micromeritics Chemisorb 2720 system was also used to conduct the hydrogen TPR studies. About 0.100 g of catalyst sample was swept with 50 mL/min He at 200 °C for 1 h in order to remove the impurities. Next, the catalyst samples were reduced using a 5 % H_2/Ar mixture at a heating rate of 10 °C/min in a temperature range of 30–750 °C" [19].

The experimental reaction system consisted of a gas conditioning unit, a FT-IR type CO detector (supplied by Terralab) and a stainless steel tubular reactor inserted in a tubular furnace connected to the Hiden Analytical Model HPR20 3F R&D Mass Spectrometer (MS). In the gas conditioning unit, liquid ethanol was vaporized in a gas washing bottle inserted in a heated chamber at 35 °C. The carrier gas helium bubbled through the gas washing bottle, carrying the formed ethanol vapor with it. Later, in the same chamber, the helium and ethanol mixture was combined with the oxygen gas and sent to the CO FT-IR detector. The flow rates of helium and oxygen were controlled by the mass flow meters mounted on the gas conditioning unit. In order to calculate and adjust the flow rate of the ethanol vapor, the Antoine equation was used by also considering the lower flammability and upper flammability limits (LFL and UFL) of the reaction mixture so that the amount of oxygen (hence the O_2/EtOH molar ratio) would be sufficient to sustain the oxidation reaction but not too much to yield excessive CO_2, and H_2O as byproducts. The gas mixture leaving the gas conditioning unit was sent to the FT-IR type CO detector in order to determine the CO concentration in the product stream since the mass spectrometer could not precisely differentiate between the CO and CO_2 gases. The reaction mixture leaving the detector was sent to a stainless steel tubular reactor, and all the transfer lines in the reaction system were heated to 120 °C using electrical heaters to prevent any condensation. A catalyst mass of 0.200 g was used in the tubular reactor. The reaction mixture that left the reactor was analyzed by the MS to obtain the product distribution. The reactions were carried out at a total (helium + ethanol vapor + oxygen) constant gas flow rate of 50 ml/min or a space velocity of 2206 h^{-1} for 16 h.

2.1. Synthesis of the SBA-15 catalyst

For the synthesis of the SBA-15 type catalyst, the recipe given by Zhao et al. [20] was used with some modifications in the gelation, washing, drying and calcination stages. First of all 4 g of Pluronic® P123 (Aldrich) and 2.2 g of HCl (Merck, 37 %) were dissolved in distilled water at 35 °C by continuous stirring for 16 h. Then, 7.9 g of TEOS (Fluka, ≥99,0 %) was added to this solution dropwise by continuous stirring and the stirring was continued for 24 h more at 35 °C so that the SBA-15 structure may form. After this stage, the solution was transferred to a Teflon bottle and kept in an oven for 24 h at 100 °C and the product from the oven was filtered and washed

using a vacuum pump until the pH of the filtrate was 7.00. The washed product was dried slowly at room temperature for about three days. Finally, the dried product was calcined by heating from room temperature to 550 °C under a dry air flow of 1 L/min by a heating rate of 1 °C/min and keeping at this temperature for 6 h in a quartz cylindrical calcination tube with a quartz membrane in the middle designed by the researchers.

2.2. Synthesis of Pd-SBA-15-IMP catalysts

The Pd-SBA-15-IMP catalysts were synthesized using the recipe given by Fukuoka et al. [21] for H_2PdCl_4-HMM-1 with some modifications: For the synthesis of 1 g of 3%Pd-SBA-15-IMP catalyst; 51.5 miligram of $PdCl_2$ was dissolved in 4.056 g of HCl to obtain H_2PdCl_4. Simultaneously, the previously synthesized SBA-15 catalyst was cleaned under vacuum (in the degas unit of the Micromeritics ASAP 2020 system) for 10 h at 150 °C to get rid of any moisture or physical impurities attached to its surface. After degassing, 1 g of the degassed sample was dissolved in 30 ml of distilled water, and in a separate beaker the H_2PdCl_4 was dissolved in 20 ml of distilled water. Then, the H_2PdCl_4 solution was added dropwise to the SBA-15 solution with continuous stirring, so palladium would diffuse into the SBA-15 pores. The solution thus formed was inserted into an oven pre-heated to 60 °C and remained in the oven until all the water evaporated. Finally, the solid product (H_2PdCl_4-SBA-15) was calcined at 500 °C under a dry air flow of 1 L/min by a heating rate of 1 °C/min and keeping at this temperature for 6 h in the quartz calcination tube to yield the Pd-SBA-15-IMP catalysts. Literature results show that when a similar recipe is used for the wet impregnation synthesis of Pd-MCM-41, the H_2PdCl_4-MCM-41 material is converted into PdO-MCM-41 upon calcination [22]. The 1%Pd-SBA-15-IMP and 5%Pd-SBA-15-IMP catalysts were synthesized in a similar way making sure that the Pd/Si molar ratio in the solution was 1.0 and 5.0, respectively.

3. Results and discussion

In order to better understand the physicochemical properties and the crystal structure of the as-synthesized catalysts, XRD analysis was used. SBA-15 has a two-dimensional, hexagonal, through-hole structure with a space group p6mm [23]. It shows three XRD diffraction peaks, which can be assigned to (100), (110) and (200) crystal face diffractions [24]. These peaks are obtained in the 2θ range of 0.5–3.0°, with the primary (100) peak around at 1° and the two secondary peaks (110) and (200) around 1.6° and 1.9°, respectively [25]. The XRD patterns given in Fig. 1(a and b) depict that the characteristic SBA-15 structure was obtained for the purely siliceous sample and preserved for the Pd-SBA-15-IMP samples upon addition of the palladium metal, as seen from the secondary peaks around 1.6 and 1.9°, which indicate long-range order and hexagonal pore shapes (the primary peak was not precisely obtained due to the limitations of the diffractometer) [23–25]. Considering Fig. 1(b), for the 1%Pd-SBA-15-IMP catalyst, no Pd or PdO peak was obtained. For the 3%Pd-SBA-15 catalyst only the (101) peak of PdO was obtained around 35° with a low intensity. The fact that the PdO (101) peak was present with low intensities and there were no other detectable peaks for this catalyst illustrated that part of the palladium loaded had been incorporated into the mesopores or embedded into the silica walls as small particles [26,27], while part of it had formed PdO crystallites on the outside surfaces of the catalyst particles. For the 5%Pd-SBA-15-IMP catalyst, both the (101) and (110) peaks of PdO were obtained around 35 and 45° [28] and the intensity of the (101) peak was higher than that of 3%Pd-SBA-15, indicating the formation of more PdO crystallites on the outer surface of the catalyst. Finally, the wide band centered around $2\theta = 23°$ corresponds to the presence of amorphous silica (silica walls) with a stable structure [29].

In order to determine the metal distribution, the metal surface area and the active particle size, CO chemical sorption analysis was carried out. As seen in Table 1, palladium metal was successfully incorporated into all catalysts. The largest active particle size was seen to occur at 3 % metal loading. The metal distribution values in Table 1 show the ratio of the metal that is incorporated into the surface of the catalyst to the total amount of metal found in the catalyst. As seen in Table 1, metal distribution values were low in the

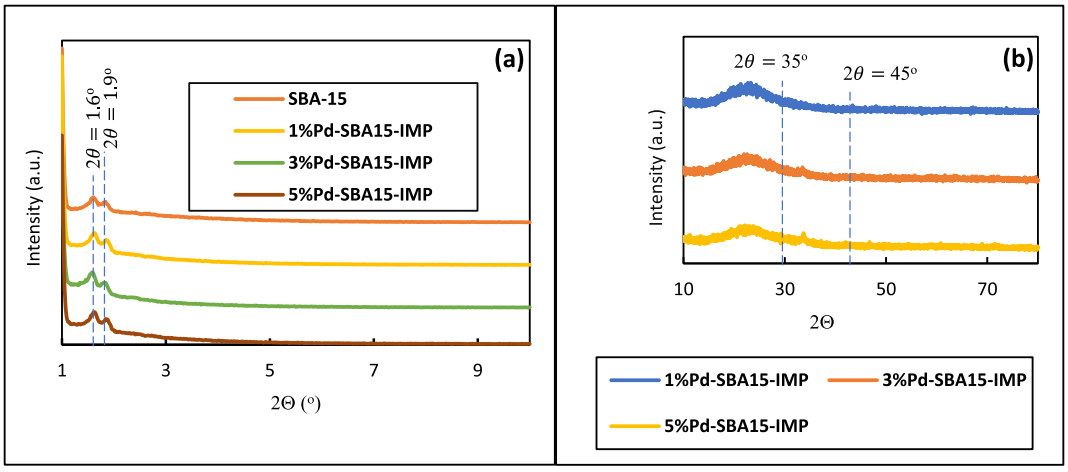

Fig. 1. XRD patterns of the SBA-15 and SBA-15-IMP catalysts (a) Low angle range of 1-10° (b) Wide angle range of 10-80.°

Table 1
Chemisorption results of SBA-15 and Pd-SBA-15-IMP catalysts.

Sample	Metal Distribution (%MD)	Metal Surface Area		Active particle (PdO) size (nm)
		m^2/g sample	m^2/g metal	
%1Pd-SBA-15-IMP	27.57	1.23	122.82	4.06
%3Pd-SBA-15-IMP	24.02	3.21	107.01	4.66
%5Pd-SBA15-IMP	29.27	6.52	130.38	3.83

range of 24–29 % and metal surface area values were high in the range of 107–130 m^2/g, respectively [30]. The lowest metal distribution was found for the 3%Pd-SBA-15-IMP catalyst, and this indicates that this catalyst had less accessible palladium oxide species, i.e., palladium oxide incorporated in mesopores or embedded in silica walls as small particles [26], compared to other catalysts.

The surface area, pore size, and pore volume values of catalysts significantly affect their catalytic activities; hence, they need to be determined in order to interpret the reaction results effectively. For this purpose, the as-synthesized catalysts were characterized by the N_2 physisorption method. All catalysts were found to have Type IV isotherms with Type 1 hysteresis loops (not shown here). The BET surface areas, mesoporous surface areas, microporous surface areas, average BJH desorption pore diameters, DA micropore diameters, total pore volumes, DR micropore volumes and micropore volume percentages of the catalysts were also evaluated and tabulated in Table 2. As seen in Table 2, upon metal incorporation, the surface areas, pore volumes and pore diameters in general showed a decreasing trend compared to the purely siliceous SBA-15 catalyst except for the BJH desorption pore diameters which in general had an increasing trend with increasing metal content due to the fact that some of the PdO was incorporated into the silica walls [26,27] enlarging the SBA-15 infrastructure. The BET surface areas of the metal incorporated samples were significantly lower [31,32] than the purely siliceous Pd-SBA-15 due to the partial blockage of the pores upon metal addition [33]. However, the total pore volumes of the catalysts did not decrease significantly upon addition of the palladium metal; hence, it was concluded that most of the PdO particles were either embedded in the amorphous silica walls as small particles [26] or formed PdO crystallites on the outside surfaces of the SBA-15 catalysts [34].

SBA-15, contains micropores within the walls of primary mesopores forming 3-D connected pore networks [35–37] with connections between mesopores. Micropores form bridges between mesopores promoting inter-connectivity [38]. The wall porosity may increase the adsorption capacity of the SBA-15 type materials due to the increase in total surface area and enhance molecular transport of small molecules due to the interconnections [39,40]. However, micropores limit the transfer of "bulkier" molecules and result in mass transfer restrictions. In addition, microporosity increases the thermal stability of the as-synthesized SBA-15 type catalysts [41]. In contrast to zeolites, which are microporous materials, mesoporous silicas such as SBA-15 have more open structures and less thermodynamic stability than the zeolite frameworks [42]. Zhang et al. [41] found that SBA-15 materials with more micropores showed better stability in pure steam at 600 °C. Considering these discussions and Table 2, the 1%Pd-SBA-15 and 3%Pd-SBA-15 catalysts which have close microporous surface areas, same micropore volumes and close microporous volume percentages are more stable and have a larger adsorption capacity than the 5%Pd-SBA-15 catalyst which has less microporosity.

In order to have an idea about the surface characteristics, particle shapes and distributions of the as-synthesized catalysts, SEM photographs were taken at different magnification levels and given in Fig. 2(a–f). An investigation of the SEM pictures of the Pd-SBA-15-IMP catalysts shows that all of them had, in varying degrees, the thread like particle shape morphology of the SBA-15 material, but the structure was significantly destroyed for the 5%Pd-SBA-15-IMP catalyst and large clusters of PdO were formed on the outside surface of the catalyst. In addition, the distance between the particles increase as the metal loading ratio in the solution increased resulting in macropores.

Finally, the TPR characterization of the as-synthesized catalysts was performed by using the Micromeritics Chemisorb 2720 system and the results are given in Fig. 3(a–c). The peaks obtained around 150 °C for the 3%Pd-SBA-15-IMP and 5%Pd-SBA-15-IMP catalysts depict the reduction of Pd(II) species [43,44]. The band obtained around 500 °C, for the same catalysts, indicate the condensation reactions between the surface silanol groups of SBA-15 and the metal source during hydrothermal treatment [45]. The weak peak and the band obtained around 350 °C for the 1%Pd-SBA-15-IMP and 3%Pd-SBA-15 catalysts, respectively can also be attributed to the reduction of Pd(II) species to metallic palladium [46].

After completing the characterization experiments, the catalytic activities of the Pd-SBA-15-IMP catalysts were tested in the one pot oxidative synthesis of ethyl acetate at different O_2/EtOH ratios in the range of 0.2–0.8 and temperatures in the range of 100–250 °C at a space velocity of 2206 h^{-1}.

During the characterization studies, it was seen that the optimum Pd/Si molar ratio in solution was 0.03 since the 3%Pd-SBA-15-

Table 2
N_2 physisorption results of the SBA-15 and Pd-SBA-15-IMP catalysts.

Sample	Surface Area (m^2/g)			Pore Diameter (nm)		Pore Volume (cm^3/g)		
	S_{BET}	$S_{\mu,DR}$	$S_{m,BJH}$	d_{BJH}	d_{DA}	V_t	$V_{\mu,DR}$	Micropore Vol %
SBA-15	830.4	771.6	663.9	5.31	1.71	1.13	0.38	33.48
%1Pd-SBA-15-IMP	664.7	607.2	603.5	5.22	1.68	0.93	0.29	31.55
%3Pd-SBA-15-IMP	647.9	592.7	623.2	5.42	1.68	0.95	0.29	30.33
%5Pd-SBA-15-IMP	626.0	567.6	640.4	5.48	1.68	0.94	0.27	29.12

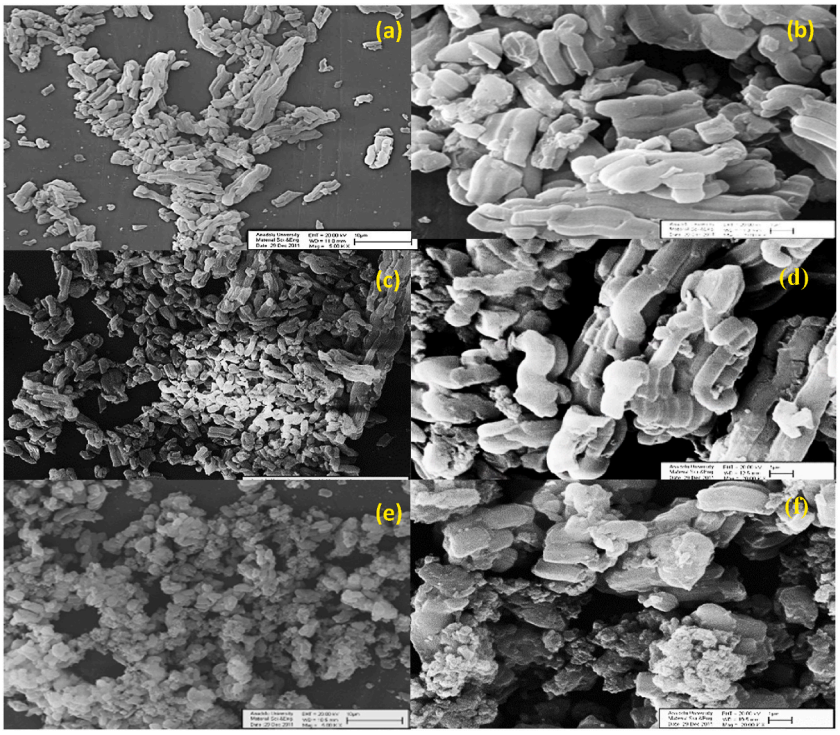

Fig. 2. SEM Photos of Pd-SBA-15-IMP catalysts (a) 1%Pd-SBA-15-IMP at 5000X magnification (b) 1%Pd-SBA-15-IMP at 20000X magnification (c) 3%Pd-SBA-15-IMP at 5000X magnification (d) 3%Pd-SBA-15-IMP at 20000X magnification (e) 5%Pd-SBA-15-IMP at 5000X magnification (f) 5%Pd-SBA-15-IMP at 20000X magnification.

IMP catalyst had a high BET surface area (~ 648 m^2/g), a high BJH desorption pore diameter (5.42 nm), less PdO crystallite formation on the outside surface of its particles and the highest total pore volume (0.95 cm^3/g) among all palladium incorporated catalysts. Hence, reaction studies were carried out using this catalyst. The 5%Pd-SBA-15-IMP catalyst was not preferred although it had a higher metal distribution, a higher metal surface area and a smaller active particle size than the 3%Pd-SBA-15-IMP catalyst, since its XRD pattern illustrated that most of the incorporated palladium formed PdO crystallites on the outside surface of its particles and since its SEM pictures depicted more structural deterioration and agglomeration compared to 3%Pd-SBA-15-IMP.

Using the 3%Pd-SBA-15-IMP catalyst and considering the LFL and UFL of the reaction mixture, first of all, the optimum O_2/EtOH molar ratio was determined. Equation (1) depicts the main reaction of ethyl acetate formation, while Fig. 4(a–f) displays the results of the reaction experiments in terms of EtOH conversion, selectivity and yield values. The conversion and selectivity values were calculated using a dry basis making a carbon atom balance and disregarding the product water. The conversion was calculated as the moles of EtOH converted into carbon based products divided into the moles of EtOH fed to the reactor system times the stoichiometric factor. The selectivity of the component *i,* on the other hand, was calculated by dividing the moles of product *i* formed into total number of moles of carbon containing products formed times the stoichiometric factor. The stoichiometric factor for component *i* was defined as the moles of EtOH required to produce 1 mol of product *i*. Finally, the yields were calculated by multiplying the conversion and selectivity values. The mechanism for the oxidative production of ethyl acetate was reported for Pd/SiO_2 type catalysts by Gaspar et al. [47] as follows: 1. Ethanol is oxidized to ethyl acetate by using the lattice oxygen of PdO. 2. Reaction of acetaldehyde with ethanol or ethoxy species followed by a dehydrogenation reaction produces ethyl acetate. 3. Acetaldehyde is oxidized to acetic acid by the O of the PdO lattice (minor amounts of acetic acid were detected in our reactions) (4) Acetaldehyde or acetic acid is oxidized to CO_2 by the O of the PdO lattice (5) PdO is reoxidized by oxygen. Considering plots 4.b, 4.d and 4.f, it is seen that ethylene yield decreases with increasing O_2/EtOH molar ratio. This behaviour shows that the reactant oxygen is not used in the formation of ethylene. Hence, ethylene can be formed by the dehydration of ethanol, given in Equation (2), which does not require gas phase oxygen and not by an oxidative dehydrogenation reaction step which requires gas phase oxygen. However, the reaction mechanism requires further justification by future mechanistic studies (such as DRIFTS studies) involving the detection of the surface intermediates during the reaction [48]. Combustion reactions are also expected at especially excess O_2 conditions as given by Equations (3) and (4).

Fig. 4(a and b) illustrates that significant ethylene formation was detected at the lean or sub-stoichiometric O_2/EtOH molar ratio of 0.2 at the lower temperatures of 100 and 150 °C with

$$C_2H_5OH\,(g) + \frac{1}{2}\,O_2\,(g) \leftrightarrow C_2H_4O\,(g) + H_2O\,(g) \quad (1)$$

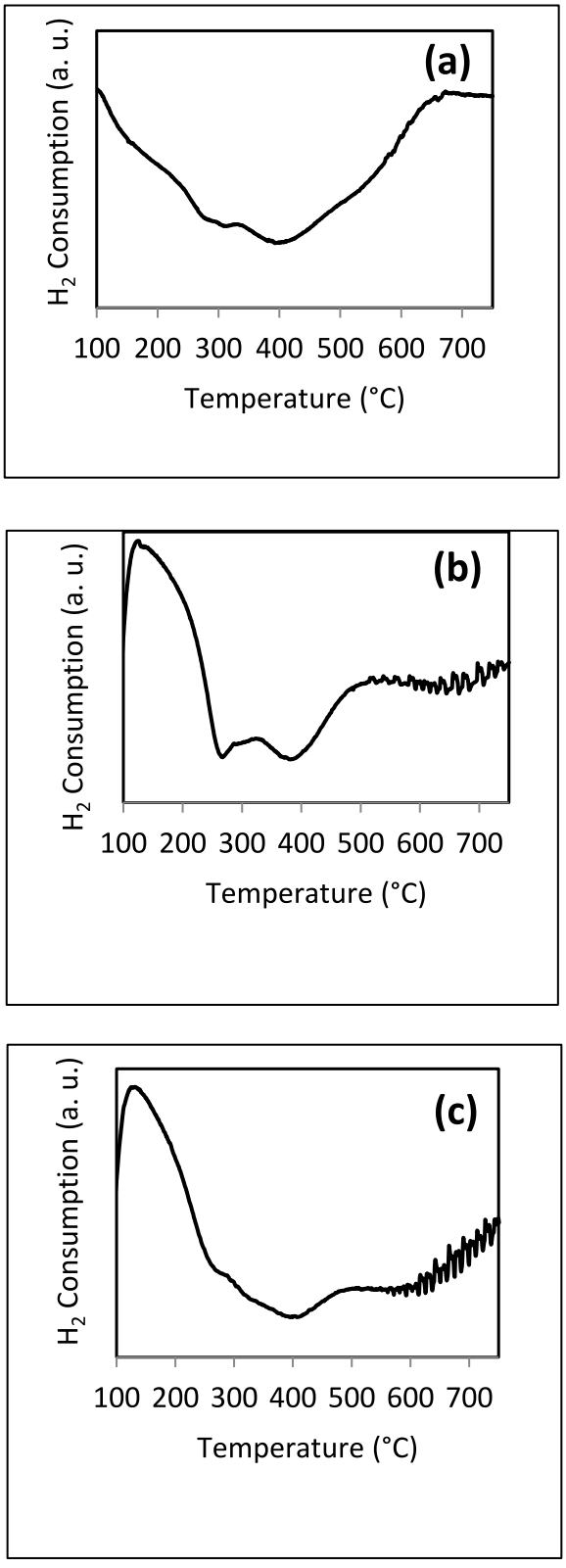

Fig. 3. TPR Profiles of SBA-15 and Pd-SBA-15 catalysts (a) 1%Pd-SBA-15-IMP (b) 3%Pd-SBA-15-IMP (c) 5%Pd-SBA-15-IMP.

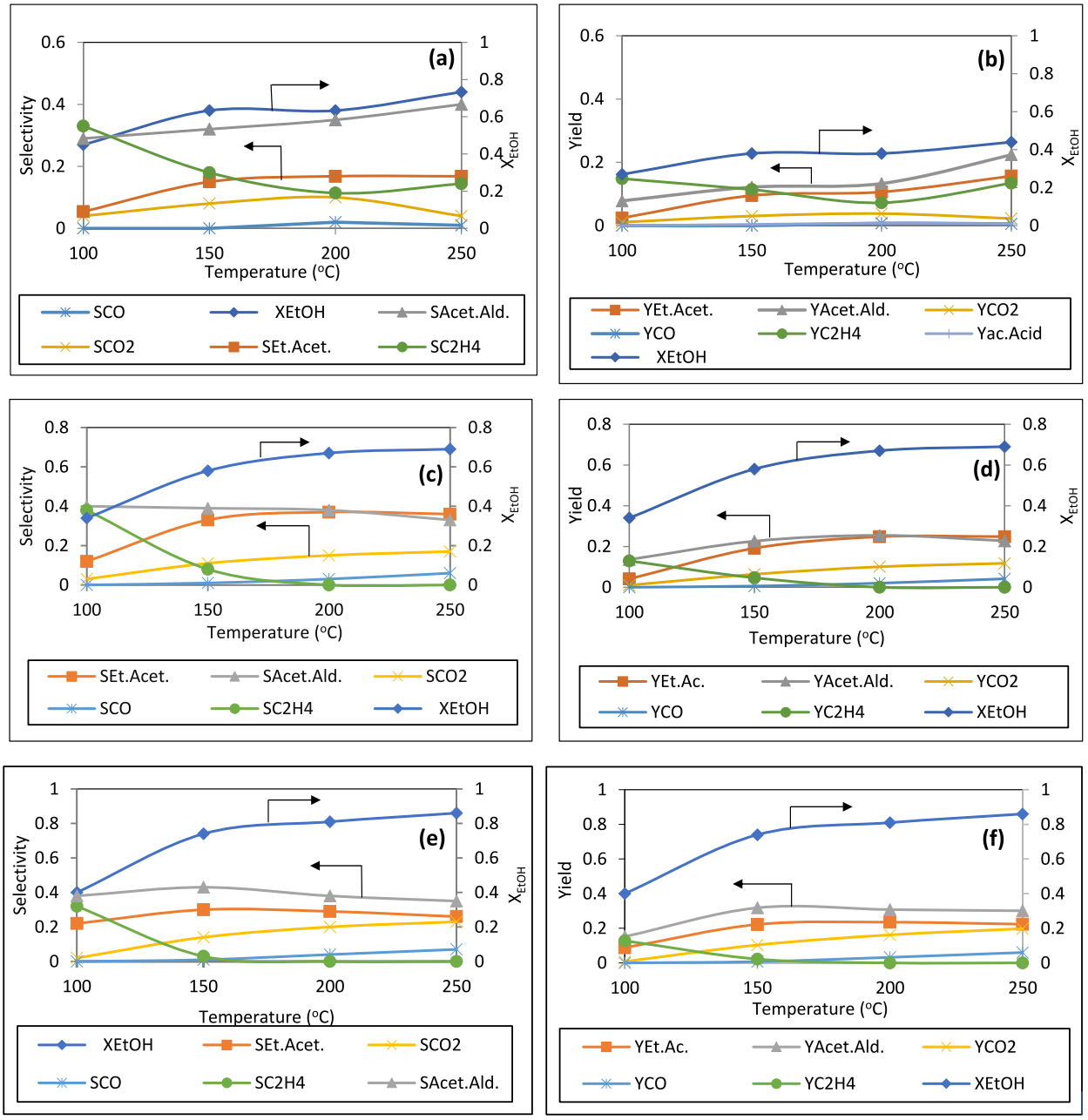

Fig. 4. Product selectivities and yields obtained at different reaction temperatures, different O_2/EtOH molar ratios and a space velocity of 2206 h^{-1} (a) Selectivities for O_2/EtOH = 0.2 (b) Yields for O_2/EtOH = 0.2 (c) Selectivities for O_2/EtOH = 0.5 (d) Yields for O_2/EtOH = 0.5 (e) Selectivities for O_2/EtOH = 0.8 (f) Yields for O_2/EtOH = 0.8.

$$C_2H_5OH\,(g) \rightarrow C_2H_4\,(g) + H_2O\,(g) \quad (2)$$

$$C_2H_5OH\,(g) + 2O_2\,(g) \rightarrow 2\,CO\,(g) + 3H_2O\,(g) \quad (3)$$

$$C_2H_5OH\,(g) + 3O_2\,(g) \rightarrow 2\,CO_2\,(g) + 3H_2O\,(g) \quad (4)$$

selectivities (S_{C2H4}) of 0.35 and 0.17, respectively, due to the dehydration of ethanol. At this oxygen ratio, the oxygen supply was insufficient to oxidize ethanol into ethyl acetate, and the oxidative dehydrogenation product acetaldehyde was primarily produced [47–49]. The maximum yield of ethyl acetate, $Y_{Et.Acet.}$, obtained was 0.13 at 250 °C. Passing from lean oxygen conditions to the stoichiometric case for which the O_2/EtOH molar ratio was 0.5, ethyl acetate selectivities and yields increased, as depicted in Fig. 4(c

and d). However, transitioning from stoichiometric conditions to the excess oxygen case (to an O_2/EtOH molar ratio of 0.8) resulted in a decrease in the ethyl acetate selectivity. This was due to the increased selectivity of acetaldehyde part of which oxidized to CO_2 and increased importance of the total combustion reaction leading to the production of more carbon dioxide, as illustrated in Fig. 4(e and f).

Considering all the reaction results in Fig. 4(a–f), the optimum O_2/EtOH ratio was found to be the stoichiometric ratio of 0.5. Fig. 4 (c and d) reveals that the maximum selectivity and yield of ethyl acetate were 0.38 and 0.25, respectively, at this optimum ratio and at 200 °C. At this ratio, the formation of acetaldehyde decreased with increasing temperature, reaching to a selectivity value of 0.33 at 250 °C. The yield of CO_2 at this optimum ratio and at 200 °C was 0.10 and no ethylene formation was detected. At the same conditions, the yield of CO was only around 0.02.

Comparing these results with literature, there are only a few studies reported for the one pot oxidative synthesis of ethyl acetate from ethanol. For instance, Gaspar et al. [47,49] utilized Pd/SiO_2 and PdO/m-ZrO_2 + t-ZrO_2 catalysts for the oxidative production of ethyl acetate in two different studies. In the first study [42], they operated under lean oxygen conditions, using O_2/EtOH molar ratio of 0.33, a space velocity of 48000 h^{-1}, catalyst mass of 25 mg. They used a saturator at 10 °C, through which air passed, to generate ethanol vapors. In this study, the maximum ethyl acetate yield obtained was around 0.57 at a low Pd/Si ratio of 0.003, however, the ethanol conversion hence the ethanol yield was not reported. The second study [49] employed PdO/m-ZrO_2 + t-ZrO_2 catalysts, with Lewis acidic sides, which led to 0.48 fractional conversion and 0.68 selectivity of ethyl acetate, resulting in a yield of 0.31. Wang et al. [50] conducted a study on the oxidative esterification of ethanol using various oxide catalysts. They found that the MoO_3-Sb_2O4 catalyst produced a maximum ethyl acetate yield of 0.30 at 110 °C, without producing significant amounts of carbon dioxide. Lin et al. [51] used excess O_2 conditions, elevated pressures as high as 35 atm and obtained an ethyl acetate yield of 0.33 at 95 °C. Gucbilmez et al. [48] used mesoporous V-MCM-41 catalysts to synthesize ethyl acetate and acetaldehyde, however, the main reaction product was ethylene and ethyl acetate was obtained only as a side product with very low yields. Chen et al. [52] explored the potential of Pd nanoparticles supported by zeolites in the selective oxidation of ethanol to acetaldehyde and ethyl acetate in the gas phase. They obtained a high ethanol yield of 0.93 after a long reaction time of 73 h. The study utilized a 2Pd/HY catalyst at a temperature of 150 °C. Thus, the 3%Pd-SBA-15 catalyst used in this study had promising results since the maximum yield was obtained at mild conditions of temperature and pressure (200 °C and atmospheric pressure) and the reaction time (16 h) was less than that reported in literature [52]. In addition, in Turkey, bio-ethanol is produced form sugar beet pulp, thus, the oxidative synthesis of ethyl acetate can be made more sustainable by using sugar beet based ethanol [53–55]. However, considering the disadvantages, the acetaldehyde and CO_2 yields obtained at the optimum conditions were also high (0.23 and 0.10, respectively), meaning that the total oxidation to ethyl acetate was not complete and the combustion reaction and acetaldehyde oxidation to CO_2 was important. Due to the fact that part of the incorporated palladium formed PdO aglomers on the outside surface of the catalyst, the catalytic yield was reduced significantly, resulting in a value of 0.25 at an EtOH conversion of 0.67. Thus, the catalyst synthesis recipes must be improved further in order to obtain more isolated PdO species inserted “into” the SBA-15 matrix, higher metal areas, and better metal distributions. In addition, recycling the by-product acetaldehyde to lower its yield and decreasing the temperature of the evaporating chamber must also be considered in order to increase the ethyl acetate yield [49,50,56].

4. Conclusions

Ethyl acetate is an important green solvent and fuel additive which reduces GHG emissions, increases the octane number and stability of fuel blends. This study utilized Pd-SBA-15 type catalysts synthesized by the impregnation method to carry out one pot oxidative synthesis of ethyl acetate. This was the first time these catalysts were used in this reaction at mild conditions of ethanol vaporization at 35 °C. All the as-synthesized catalysts displayed regular XRD patterns, high BET surface areas, and high pore volumes and the optimum Pd/Si molar ratio in solution was determined as 0.03. Thus, reaction experiments were carried out with the 3%Pd-SBA-15-IMP catalyst at the optimum O_2/EtOH molar ratio of 0.5 and at a space velocity of 2206 h^{-1}. At these conditions, the maximum ethyl acetate selectivity and yield values obtained were 0.37 and 0.25, respectively, at 200 °C and 1 atm. Comparing these values with literature, it was seen that mostly literature yields were around 0.30 and above but the corresponding processes had some disadvantages like high pressure and very long reaction times. The fact that the best yield was obtained at mild conditions of temperature and pressure decreased the energy requirement of the ethyl acetate production process. In addition, in Turkey, bio-ethanol is produced from sugar beet pulp, hence, the oxidative synthesis reaction can be made more sustainable by using sugar beet based ethanol. On the other hand, considering the disadvantages of the catalysts, the formation of PdO aglomers on the outside surface of the catalyst particles decreased the yield of ethyl acetate. Thus, catalyst synthesis methods should be improved further in order to obtain isolated PdO crystallites incorporated into the SBA-15 infrastructure, higher metal areas, and better metal distributions. In addition, recycling the oxidative dehydrogenation product acetaldehyde and lowering the temperature of the evaporating chamber can also increase the ethyl acetate yields.

CRediT authorship contribution statement

Yesim Gucbilmez: Writing – review & editing, Writing – original draft, Supervision, Resources, Project administration, Methodology, Investigation, Funding acquisition, Conceptualization. **Ibrahim Calis:** Methodology, Investigation, Funding acquisition, Conceptualization.

Funding

This work was supported by the Anadolu University [Scientific Research Projects BAP 1003F97 and BAP 1106F120].

Declaration of competing interest

The authors declare that they have no known competing financial interests or personal relationships that could have appeared to influence the work reported in this paper.

References

[1] C. Löser, T. Urit, T. Bley, Perspectives for the biotechnological production of ethyl acetate by yeasts, Appl. Microbiol. Biotechnol. 98 (2014) 5397–5415, https://doi.org/10.1007/s00253-014-5765-9.
[2] M.C. Dzialo, R. Park, J. Steensels, B. Lievens, K.J. Verstrepen, Physiology, ecology and industrial applications of aroma formation in yeast, FEMS Microbiol. Rev. 41 (2017) S95–S128, https://doi.org/10.1093/femsre/fux031.
[3] A.J. Kruis, A.C. Bohnenkamp, C. Patinios, Y.M. van Nuland, M. Levisson, A.E. Mars, C. van den Berg, S.W.M. Kengen, R.A. Weusthuis, Microbial production of short and medium chain esters: enzymes, pathways, and applications, Biotechnol. Adv. 37 (2019) 107407, https://doi.org/10.1016/j.biotechadv.2019.06.006.
[4] M.K. Yeşilyurt, D. Erol, H. Yaman, Effects of using ethyl acetate as a surprising additive in SI engine pertaining to an environmental perspective, Int. J. Eng. Sci. Technol. 19 (2022) 9427–9456, https://doi.org/10.1007/s13762-021-03706-3.
[5] M. Amine, E.N. Awad, V. Ibrahim, Y. Barakat, Effect of ethyl acetate addition on phase stability, octane number and volatility criteria of ethanol-gasoline blends, Egypt, J. Petrol. 27 (2018) 567–572, https://doi.org/10.1016/j.ejpe.2017.08.007.
[6] E. Fischer, A. Speier, Darstellung der ester, Chem. Ber. 28 (1895) 3252–3258, https://doi.org/10.1002/cber.189502803176.
[7] Y. Liu, E. Lotero, Effect of water on sulfuric acid catalyzed esterification, J. Mol. Catal. Chem. 245 (2006) 132–140, https://doi.org/10.1016/J.MOLCATA.2005.09.049.
[8] G. Jyoti, A. Keshav, J. Anandkumar, S. Bhoi, Homogeneous and heterogeneous catalyzed esterification of acrylic acid with ethanol: reaction kinetics and modelling, Int. J. Chem. Kinet. 50 (2018) 370–380, https://doi.org/10.1002/kin.21167.
[9] T. Seki, T. Nakajo, M. Onaka, The Tishchenko reaction: a classic and practical tool for ester synthesis, Chem. Lett. 35 (2006) 824–829, https://doi.org/10.1246/cl.2006.824.
[10] B.N. Pattanaik, H.C. Mandalia, Ethyl acetate: properties, production processes and applications, IJCRR 3 (2011) 23–40, 10.0.1000/xyz123/123.
[11] Z.W. Seh, J. Kibsgaard, C.F. Dickens, I. Chorkendorff, J.K. Nørskov, T.F. Jaramillo, Combining theory and experiment in electrocatalysis: insights into materials design, Science 355 (2017) eaad4998, https://doi.org/10.1126/science.aad4998.
[12] S.O. Hwang, Y.H. Park, Gas phase ethyl acetate production in a batch bioreactor, Bioprocess Eng. 17 (1997) 51–54.
[13] G. Carta, J.L. Gainer, A.H. Benton, Enzymatic synthesis of esters using an immobilized lipase, Biotechnol. Bioeng. 37 (1991) 1004–1009, https://doi.org/10.1002/bit.260371104.
[14] M. Aghazadeh, M.R. Ladisch, A.S. Engelberth, Acetic acid removal from corn stover hydrolysate using ethyl acetate and the impact on Saccharomyces cerevisiae bioethanol fermentation, Biotechnol. Prog. 32 (2016) 929–937, https://doi.org/10.1002/btpr.2282.
[15] B. Šulgan, J. Labovský, Z. Labovská, Multi-aspect comparison of ethyl acetate production pathways: reactive distillation process integration and intensification via mechanical and chemical approach, Processes 8 (2020) 1618, https://doi.org/10.3390/pr8121618.
[16] M. Klöker, E.Y. Kenig, A. Górak, A.P. Markusse, G. Kwant, P. Moritz, P, Investigation of different column configurations for the ethyl acetate synthesis via reactive distillation, Chem. Eng. Process 43 (2004) 791–801, https://doi.org/10.1016/S0255-2701(03)00084-9.
[17] K.C. Wu, Y.W. Chen, An efficient two-phase reaction of ethyl acetate production in modified ZSM-5 zeolites, Appl. Catal., A 257 (2004) 33–42, https://doi.org/10.1016/j.apcata.2003.07.014.
[18] H. Sun, Z. Qu, J. Yu, H. Ma, B. Li, D. Sun, Y. Ge, Asymmetric 5-sulfosalicylic acid-PVA catalytic pervaporation membranes for the process intensification in the synthesis of ethyl acetate, Sep. Purif. Technol. 282 (2022) 120113, https://doi.org/10.1016/j.seppur.2021.120113.
[19] Y. Gucbilmez, I. Calis, I, Effect of metal loading on the physicochemical properties of palladium oxide activated SBA-15 type mesoporous materials, in: Ö. K. Küçüksolak, C.E. Boukhedimi, T. Fırat (Eds.), International "Başkent" Congress on Physical, Social and Health Sciences Proceedings Book, ISCYA YAYINEVİ®, 2021, pp. 153–162. TURKEY, USA, 2021.
[20] D. Zhao, J. Feng, Q. Huo, N. Melosh, G.H. Fredrickson, B.F. Chmelka, G.D. Stucky, Triblock copolymer syntheses of mesoporous silica with periodic 50 to 300 angstrom pores, Science 279 (1998) 548–552, https://doi.org/10.1126/science.279.5350.548.
[21] A. Fukuoka, H. Araki, Y. Sakamoto, S. Inagaki, Y. Fukushima, M. Ichikawa, Palladium nanowires and nanoparticles in mesoporous silica templates, Inorg. Chim. Acta. 350 (2003) 371–378, https://doi.org/10.1016/S0020-1693(02)01541-4.
[22] C. Şener, Synthesis and Characterization of Pd-MCM-type Mesoporous Nanocomposite Materials, 2006. Ankara.
[23] A.S. Maria Chong, X.S. Zhao, Functionalization of SBA-15 with APTES and characterization of functionalized materials, JPCB 107 (2003) 12650–12657, https://doi.org/10.1021/jp035877+.
[24] ACS Materials, American chemicals supplier. https://www.acsmaterial.com/blog-detail/sba-15-mesoporous-molecular-sieve.html?srsltid=AfmBOoqcvUw-SUa-NnwangOmqOBt2b1WFSLhMLXevGc5B7skPF4zedbO, 2024. (Accessed 3 January 2025).
[25] S.M. El-Sheikh, Adel A. Ismail, Jafar F. Al-Sharab, Catalytic reduction of P-Nitrophenol over precious metals/highly ordered mesoporous silica, New J. Chem. 37 (2013) 2399–2407. https://pubs.rsc.org/en/content/articlelanding/2013/nj/c3nj00138e.
[26] A. Solmaz, S. Balci, T. Dogu, Synthesis and characterization of V, Mo and Nb incorporated micro–mesoporous MCM-41 materials, Mater. Chem. Phys. 125 (2011) 148–155, https://doi.org/10.1016/j.matchemphys.2010.08.086.
[27] Z. Lou, R. Wang, H. Sun, Y. Chen, Y. Yang, Direct synthesis of highly orderedCo-SBA-15 mesoporous materials by the pH-adjusting approach, Microporous Mesoporous Mater. 110 (2008) 347–354, https://doi.org/10.1016/j.micromeso.2007.06.020.
[28] J. Yan, X. Li, B. Jin, M. Zeng, R. Peng, Synthesis of TiO_2/Pd and TiO_2/PdO hollow spheres and their visible light photocatalytic activity, Int. J. Photoenergy (2020) 1–9, https://doi.org/10.1155/2020/4539472.
[29] M. Ulfa, H. Al Afif, T.E. Saraswati, H. Bahruji, Fast removal of methylene blue via adsorption-photodegradation on TiO_2/SBA-15 synthesized by slow calcination, Mater 15 (2022) 5471, https://doi.org/10.3390/ma15165471.
[30] K. Belkacemi, A. Boulmerka, J. Arul, S. Hamoudi, Hydrogenation ofvegetable oils with minimum trans and saturated fatty acid formation over a new generationof Pd-catalyst, Top. Catal. 37 (2006) 113–120, https://doi.org/10.1007/s11244-006-0012-y.
[31] D. Vargas-Hernández, J.M. Rubio-Caballero, J. Santamaría-González, R. Moreno-Tost, J.M. Mérida-Robles, M.A. Pérez-Cruz, M. A, et al., Furfuryl alcohol from furfural hydrogenation over copper supported on SBA-15 silica catalysts, J. Mol. Catal. Chem. 383 (2014) 106–113, https://doi.org/10.1016/j.molcata.2013.11.034.
[32] C. Salameh, J.P. Nogier, F. Launay, M. Boutros, Dispersion of colloidal TiO_2 nanoparticles on mesoporous materials targeting photocatalysis applications, Catal. Today 257 (2015) 35–40, https://doi.org/10.1016/j.cattod.2015.03.025.
[33] N.S. Ali, Z.T. Alismaeel, H.S. Majdi, H.G. Salih, M.A. Abdulrahman, N. Saady, T.M. Albayati, Modification of SBA-15 mesoporous silica as an active heterogeneous catalyst for the hydroisomerization and hydrocracking of n-heptane, Heliyon 8 (2022) e09737, https://doi.org/10.1016/j.heliyon.2022.e09737.
[34] M. Can, B. Akça, A. Yilmaz, D. Üner, Synthesis and characterization of Co-Pb/SBA-15 mesoporous catalysts, Turk. J. Phys. 29 (2005) 287–294.

[35] R. Ryoo, C. Hyun Ko, M. Kruk, V. Antochshuk, M. Jaroniec, Block-copolymer-templated ordered mesoporous silica: array of uniform mesopores or mesopore-micropore network? J. Phys. Chem. B 104 (2000) 11465–11471, https://doi.org/10.1021/jp002597a.
[36] S. Jun, S.H. Joo, R. Ryoo, M. Kruk, M. Jaroniec, Z. Liu, T. Ohsuna, O. Terasaki, Synthesis of new, nanoporous carbon with hexagonally ordered mesostructure [5], J. Am. Chem. Soc. 122 (2000) 10712–10713, https://doi.org/10.1021/ja002261e.
[37] S.H. Joo, R. Ryoo R., M. Kruk, M. Jaroniec, Evidence for general nature of pore interconnectivity in 2-dimensional hexagonal mesoporous silicas prepared using block copolymer templates, J. Phys. Chem. B 106 (2002) 4640–4646, https://doi.org/10.1021/jp013583n.
[38] A. Galarneau, H. Cambon, F. Di Renzo, R. Ryoo, M. Choi, F. Fajula, Microporosity and connections between pores in SBA-15 mesostructured silicas as a function of the temperature of synthesis, New J. Chem. 27 (2003) 73–79, https://doi.org/10.1039/B207378C.
[39] L. Vradman, L. Titelman, M. Herskowitz, Size effect on SBA-15 microporosity, Microporous Mesoporous Mater. 93 (2006) 313–317, https://doi.org/10.1016/j.micromeso.2006.03.014.
[40] B.L. Newalkar, N.V. Choudary, U.T. Turaga, R.P. Vijayalakshmi, P. Kumar, S. Komarneni, T.S.G. Bhat, Potential adsorbent for light hydrocarbon separation: role of SBA-15 framework porosity, Chem. Mater. 15 (2003) 1474–1479, https://doi.org/10.1021/cm020889d.
[41] F. Zhang, Y. Yan, H. Yang, Y. Meng, C. Yu, B. Tu, D. Zhao, Understanding effect of wall structure on the hydrothermal stability of mesostructured silica SBA-151, J. Phys. Chem. B 109 (2005) 8723–8732, https://doi.org/10.1021/jp044632+.
[42] O. Trofymluk, A.A. Levchenko, A.I. Navrotsky, Mesoporous silica synthesis: energetics of interaction between framework and structure directing agent, Microporous Mesoporous Mater. 149 (2012) 119–125, https://doi.org/10.1016/j.micromeso.2011.08.022.
[43] Y. Liu, T. Hayakawa, T. Ishii, M. Kumagai, H. Yasuda, K. Suzuki, et al., Methanol decomposition to synthesis gas at low temperature over palladium supported on ceria-zirconia solid solutions, Appl. Catal. Gen. 210 (2001) 301–314, https://doi.org/10.1016/S0926-860X(00)00817-6.
[44] A. Sarkany, Z. Zsoldos, G. Stefler, J.W. Hightower, L. Guczi, Promoter effect of Pd in hydrogenation of 1,3-butadiene over Co-Pd catalysts, J. Catal. 157 (1995) 179–189, https://doi.org/10.1006/jcat.1995.1278.
[45] Y. Park, T. Kang, P. Kim, J. Yi, Encapsulation method for the dispersion of NiO onto ordered mesoporous silica SBA-15, using polyethylene oxide (PEO), J. Colloid Interface Sci. 295 (2006) 464–471, https://doi.org/10.1016/j.jcis.2005.09.006.
[46] Q. Zheng, R. Farrauto, M. Deeba, Part II: oxidative thermal aging of Pd/Al_2O_3 and $Pd/CexOy\text{-}ZrO_2$ in automotive three way catalysts: the effects of fuel shutoff and attempted fuel rich regeneration, Catalysts 5 (2015) 1797–1814, https://doi.org/10.3390/catal5041797.
[47] A. Gaspar, A. Esteves, F. Mendes, F. Barbosa, L. Appel, Chemicals from ethanol—the ethyl acetate one-pot synthesis, Appl. Catal. Gen. 363 (2009) 109–114, https://doi.org/10.1016/j.apcata.2009.05.001.
[48] Y. Gucbilmez, T. Dogu, S. Balci, Ethylene and acetaldehyde production by selective oxidation of ethanol using mesoporous V−MCM-41 catalysts, Ind. Eng. Chem. Res. 45 (2006) 3496–3502, https://doi.org/10.1021/ie050952j.
[49] A.B. Gaspar, F.G. Barbosa, S. Letichevsky, L.G. Appel, Chemicals from ethanol-the ethyl acetate one-pot synthesis. 21st North American Catalysis Society Meeting, 2009. San Francisco, USA.
[50] L. Wang, K. Eguchi, H. Arai, T. Seiyama, Oxidative esterification of ethanol over oxide catalysts, Chem. Lett. 15 (1986) 1173–1176, https://doi.org/10.1246/cl.1986.1173.
[51] T.-B. Lin, D.-L. Chung, J.-R. Chang, J-R, Ethyl acetate production from water-containing ethanol catalyzed by supported Pd catalysts: advantages and disadvantages of hydrophobic supports, Ind. Eng. Chem. Res. 38 (1999) 1271–1276, https://doi.org/10.1021/ie9805887.
[52] H. Chen, Y. Dai, X. Jia, H. Yu, Y. Yang, Highly selective gas-phase oxidation of ethanol to ethyl acetate over bi-functional Pd/zeolite catalysts, Green Chem. 18 (2016) 3048–3056, https://doi.org/10.1039/C5GC02593A.
[53] Türkiye şeker fabrikaları anonim şirketi, Faaliyet raporu, 2015. https://www.turkseker.gov.tr/data/dosyalar/Faaliyet_Raporlari2019_12_07_11_10_32_221.pdf (Accessed 16 January 2025).
[54] S.G. Altunbay, A. Kangal, S. Gürel, Şeker pancarından biyoetanol üretimi, Tarla Bitkileri Merkez Araştırma Enstitüsü Dergisi 25 (2016) 334–339.
[55] Türkşeker, Sektör raporu, 2021. https://www.turkseker.gov.tr/data/dokumanlar/2021_Sektor_Raporu.pdf (Accessed 16 January 2025).
[56] N. Ivashchenko, W. Gac, V. Tertykh, V. Yanishpolskii, S. Khainakov, A. Dikhtiarenko, S. Pasieczna-Patkowska, W. Zawadzki, Preparation, characterization and catalytic activity of palladium nanoparticles embedded in the mesoporous silica matrices, World J. Nano Sci. Eng. 2 (2012) 117–125, https://doi.org/10.4236/wjnse.2012.23015.